ELSEVIER

Journal of Biomechanics 41 (2008) 1782–1789

JOURNAL OF BIOMECHANICS

www.elsevier.com/locate/jbiomech
www.JBiomech.com

Associating the mesoscale fiber organization of the tongue with local strain rate during swallowing

Samuel M. Felton[a,b], Terry A. Gaige[a,b], Thomas Benner[a,b], Ruopeng Wang[a,b], Timothy G. Reese[a,b], Van J. Wedeen[a,b], Richard J. Gilbert[a,b,*]

[a]*Department of Mechanical Engineering, Massachusetts Institute of Technology, 77 Massachusetts Avenue, Cambridge, MA 02139, USA*
[b]*Athinoula A. Martinos Center for Biomedical Imaging, Massachusetts General Hospital, Charlestown, MA, USA*

Accepted 17 January 2008

Abstract

The tongue is an intricately configured muscular organ that undergoes a stereotypical set of deformations during the course of normal human swallowing. In order to demonstrate quantitatively the relationship between 3D aligned lingual fiber organization and mechanics during swallowing, the tissue's myoarchitecture and strain rate were imaged before and during the propulsive phase of a 3.0 ml water bolus swallow. Mesoscale fiber organization was imaged with high-resolution diffusion tensor imaging (DTI) and multi-voxel myofiber tracts generated along maximum diffusion vectors. Tissue compression/expansion was obtained via lingual pressure-gated phase-contrast (PC) MRI, a method which determines local strain rate as a function of the phase shift occurring along an applied gradient vector. The co-alignment of myofiber tract direction and the localized principal strain rate vectors was obtained by translating the strain rate tensor into the reference frame with the primary axis parallel to the maximum diffusion vector using Mohr's circle, resulting in the generation of fiber-aligned strain rate (FASR). DTI tractography displayed the complete fiber anatomy of the tongue, consisting of a core region of orthogonally aligned fibers encased within a longitudinal sheath, which merge with the externally connected styloglossus, hyoglossus, and genioglossus fibers. FASR images obtained in the mid-sagittal plane demonstrated that bolus propulsion was associated with prominent compressive strain aligned with the genioglossus muscle combined with expansive strain aligned with the verticalis and geniohyoid muscles. These data demonstrate that lingual deformation during swallowing involves complex interactions involving intrinsic and extrinsic muscles, whose contractility is directed by the alignment of mesoscale fiber tracts.
© 2008 Published by Elsevier Ltd.

Keywords: MRI; Phase contrast; DTI; Tractography; Muscle imaging; Strain

1. Introduction

Associating microscopic fiber organization with tissue deformation is a challenging task in tissues where the constituting myofibers express complex geometries. The mammalian tongue is an apt model for such studies since its myoarchitecture is comprised by an intricate 3D network of intrinsic and extrinsic muscles (Sonntag, 1925; Wedeen et al., 2001; Napadow et al., 2001) (Fig. 1). Lingual intrinsic musculature consists of a core region of orthogonally aligned fibers, contained within a sheath-like tract of longitudinally oriented fibers. These intrinsic fibers merge with extrinsic muscles that modify shape and position from a superior (palatoglossus), posterior (styloglossus), and inferior direction (genioglossus and hyoglossus). During swallowing, the tongue undergoes a characteristic set of deformations, dictated largely by its hydrostatic properties (Smith, 1986; Smith and Kier, 1989; Napadow et al., 1999a, 2002; Gilbert et al., 2007), which serve to shape the ingested bolus (early accommodation), transfer the bolus from the anterior to the posterior oral cavity (late accommodation), and then transfer the configured bolus into the pharynx (propulsion) (Napadow et al., 1999b).

NMR methods have been developed depicting mesoscale representations of 3D fiber organization and mechanics.

*Corresponding author at: Department of Mechanical Engineering, Massachusetts Institute of Technology, 77 Massachusetts Avenue, Cambridge, MA 02139, USA. Tel.: +1 617 620 2032; fax: +1 781 622 5090.
E-mail address: rgilbert@mit.edu (R.J. Gilbert).

0021-9290/$ - see front matter © 2008 Published by Elsevier Ltd.
doi:10.1016/j.jbiomech.2008.01.030

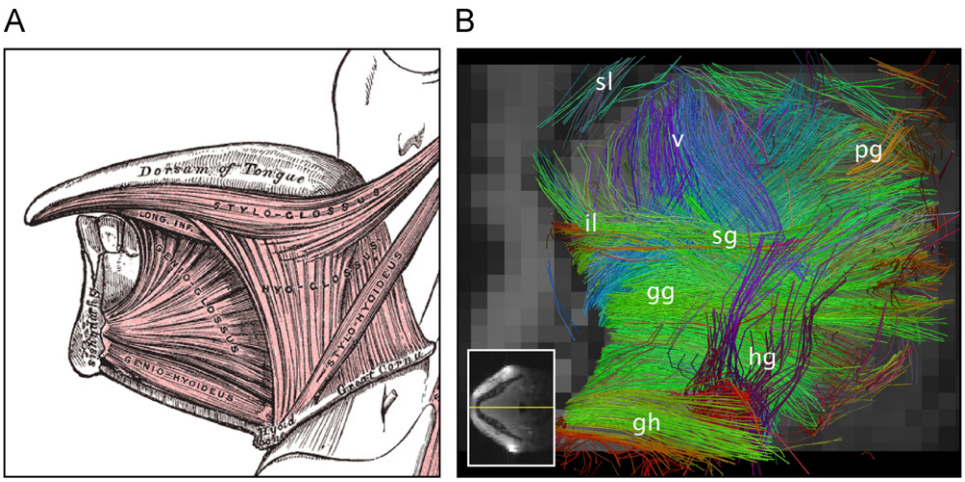

Fig. 1. Lingual muscular anatomy. The musculature of the tongue is classically divided into two types of muscle, intrinsic and extrinsic. The intrinsic muscles include the superior and inferior longitudinalis, the transversus, and the verticalis muscles. The transversus, verticalis, and longitudinalis muscles also extend to the posterior tongue, where they are merged with the extrinsic muscles. These muscles enter the tongue proper from a superior direction (palatoglossus), postero-superior direction (styloglossus), postero-inferior direction (hyoglossus) and antero-inferior direction (genioglossus). The genioglossus comprises the bulk of the posterior tongue and enters the tongue in a fan-like projection, originating at the mental spine of the mandible. The tongue rests on a muscular floor composed of the geniohyoid muscle, which runs in the mid-sagittal plane from the mental spine of the mandible to the body of the hyoid bone; and the mylohyoid, which runs from the mylohyoid line of the mandible to the raphe and body of the hyoid bone. Shown in this figure is an anatomical drawing obtained from Gray's anatomy (A) is presented in comparison to a sagittal 3D view of lingual myoarchitecture based on in vivo DTI tractography (B). Note the close structural correlation between genioglossus (gg), geniohyoid (gh), hyoglossus (hg), and styloglossus (sg) merged with the inferior longitudinalis (il). Not shown in the anatomical drawing, but generally visible in tractography images are the superior longitudinalis (sl) and verticalis (v) fibers in the anterior tongue, and the palatoglossus (pg) in the posterior tongue. Inset in left lower corner of (B) demonstrates the reference location of the MRI image.

Diffusion-weighted NMR defines myoanatomy as an array of elements representing directional differences of proton diffusion (Stejskal and Tanner, 1965), and can be used to define 3D fiber alignment in terms of principal fiber direction at the voxel (Basser et al., 1994; Wedeen et al., 2001; Napadow et al., 2001; Gilbert et al., 2006a) or multi-voxel scale in terms of myofiber tracts generated by streamline tractography (Gilbert et al., 2006b; Gaige et al., 2007). Moreover, we have employed gated phase contrast MRI (Felton et al., 2007), a method which derives directional change of compression or expansion based on the difference between adjacent velocity vectors (Dou et al., 2003; Ebbers et al., 2002; Wedeen et al., 1995) to map the distribution of local strain rate during swallowing, The goal of the current study was to merge these measures to define relationships between aligned myofiber populations and local strain rate. This approach associates the orientation of the principal diffusion vectors and the principal strain rate vectors for each voxel resulting in a measure of the deformation of the underlying fiber, termed fiber-aligned strain rate (FASR). thus deriving a mesoscale representation of local mechanical function referenced to its myoarchitecture.

2. Methods

2.1. General methods

Lingual myoarchitecture and strain rate were determined with high-resolution diffusion tensor and phase-contrast MRI in normal volunteers. Subjects ($n = 4$, 3 males, 1 female, ages 21–24) possessed no history or current abnormalities of speech or swallowing. The study was approved by the MIT Committee on the use of humans as experimental subjects.

2.2. Diffusion tensor imaging (DTI) with tractography

DTI tractography derives the orientation of fiber populations by measuring anisotropic proton diffusion at each location in a tissue (Basser et al., 1994; Wedeen et al., 2001). The physical basis by which diffusion-weighted MRI infers fiber direction in muscular tissue has been published (Wedeen et al., 2001; Napadow et al., 2001, Gilbert et al., 2006a, b, Gaige et al., 2007) and validated relative to microscopy (Napadow et al., 2001). In brief, diffusion represents the random translational motion of protons contained in water molecules and is principally modulated by the presence and location of macromolecular barriers to water displacement. The diffusion tensor depicts net proton diffusion in a volume of tissue with a symmetric 2nd rank tensor, and can be interpreted as an ellipsoid whose axes are constructed along its three orthogonal eigenvectors with each axis proportional to its eigenvalues. The application of gradients, configured as evenly spaced directions on the surface of a model sphere, results in a system of linear equations that over-constrains the components of the diffusion tensor and may be solved using multiple linear regression. Diffusion-weighted gradients were applied in 90 unique directions employing single shot echo-planar (EPI) spatial encoding and the following imaging parameters: TR = 3000 ms, TE = 80 ms, field of view 192 mm × 192 mm, 3 mm slice thickness, and a b-value of 500 s/mm^2. These parameters allowed complete acquisitions for the DTI tractography image set to be accomplished in approximately 5 min. Maximum diffusion is a vector defined as the largest eigenvector of the diffusion tensor. Multi-voxel myofiber tracts were generated along the maximum diffusion vector per voxel employing streamline construction, a method for constructing connections along the vector directions in a vector field, as previously described (Gilbert et al., 2006b). The specific method operates by applying the constraint that a certain angular threshold must be met to establish

intervoxel connectivity, and thus constitute the myofiber tract. In the current work, if the angular difference between a given streamline and the maximum diffusion vector of an adjacent voxel is less than $\pm 35^{\circ}$, intervoxel myofiber tract continuity is established.

2.3. Phase-contrast MRI (PC MRI)

The general methods for deriving strain rate from PC MRI have been previously published and validated (Felton et al., 2007; Dou et al., 2003; Ebbers et al., 2002; Wedeen et al., 1995). PC MRI determines the local (single voxel) velocity function by applying a phase gradient followed by a canceling (decoding) phase gradient, then deriving local motion by the phase shift exhibited by the resulting MR images along the gradient vector. During PC MRI, velocity encoding is applied in four quadrilateral directions: (x, y, z), $(-x,-y, z)$, $(x,-y,-z)$, $(-x, y,-z)$ and strain rate determined by the difference in velocities between adjacent voxels. Strains can be linearly approximated by the strain tensor, given by a 3×3 matrix. Individual PC images were determined to have a signal-to-noise ratio (SNR) of 48.5. Specific imaging parameters included: echo time 54 ms, repetition time 274 ms, and VENC 0.67 cm/s/cycle. One acquisition was performed in each slice per swallow. Data was acquired using two custom-built surface coils, approximately 150 mm^2 in area, placed on each cheek and secured to the skin with adhesive tape. Lagrangian strain was calculated with an unsupervised and objective algorithm developed in Mathematica. Strain rate was calculated by

$$\frac{\partial \varepsilon_{ap}}{\partial t} = \frac{(\partial a/\partial p)\mathrm{VENC}}{L}\varepsilon_{ap} = \frac{\partial u_a}{\partial p} \tag{1}$$

where L is the voxel length, VENC is the velocity encoding number, p represents any principal vector x, y, or z, and u_a is the material displacement along vector a. The relation between the four equilateral gradient vectors, a, b, c, and d, and the two principal vectors, x and y, are represented by

$$\frac{\partial \varepsilon_{xp}}{\partial t} = \left(\frac{\partial \varepsilon_{ap}}{\partial t} - \frac{\partial \varepsilon_{bp}}{\partial t} + \frac{\partial \varepsilon_{cp}}{\partial t} - \frac{\partial \varepsilon_{dp}}{\partial t}\right)\frac{\sqrt{3}}{4} \tag{2}$$

$$\frac{\partial \varepsilon_{yp}}{\partial t} = \left(\frac{\partial \varepsilon_{ap}}{\partial t} - \frac{\partial \varepsilon_{bp}}{\partial t} + \frac{\partial \varepsilon_{cp}}{\partial t} - \frac{\partial \varepsilon_{dp}}{\partial t}\right)\frac{\sqrt{3}}{4} \tag{3}$$

The orthogonal dimensions are then translated into principal strain vectors with no shear strain. In order to represent the local strain rate tensor for each voxel, the principal strain rates for the tissue contained in each voxel were rendered as 2D icons. For this study, strain rate was represented graphically using rhombi with their long dimension parallel to a strain rate eigenvector and the length proportional to its magnitude. The width of each rhombus was arbitrarily set proportional to the length for the purpose of visualization. For each voxel, two orthogonally aligned rhombi were generated representing the strain rate tensor eigenvectors, or principal strain rate vectors, of that voxel. A blue rhombus indicates a positive principal strain rate, consistent with expansion, and a red rhombus indicates a negative principal strain rate, consistent with compression. Each rhombus was overlayed in the correct position on the magnitude images of the tongue during the propulsive image sequence.

2.4. Geometric relationship between aligned strain rate and myofiber tract orientation

An objective algorithm was applied to determine FASR. Each voxel contains one maximum diffusion vector and one strain rate tensor. The strain rate tensor is transformed onto the reference plane with x-axis parallel to the diffusion vector.

$$\angle\overline{\mathrm{FASR}} = \angle\hat{d} = \theta_d \tag{4}$$

$$\left|\overline{\mathrm{FASR}}\right| = \frac{\partial \varepsilon_{x'x'}}{\partial t} = \frac{(\partial \varepsilon_{xx}/\partial t) + (\partial \varepsilon_{yy}/\partial t)}{2} + \cos(2\theta_d)\frac{(\partial \varepsilon_{xx}/\partial t) - (\partial \varepsilon_{yy}/\partial t)}{2} + \sin(2\theta_d)\frac{(\partial \varepsilon_{xy}/\partial t) - (\partial \varepsilon_{yx}/\partial t)}{2} \tag{5}$$

FASR is so defined as a local vector with units per second, parallel to its associated diffusion vector, and with magnitude equal to the axial strain rate of the parallel axis within that reference frame (Fig. 2). Fibers are portrayed as red (those exhibiting principal compression) or blue (those exhibiting principal expansion) with hue proportional to the magnitude of the local FASR. Mean FASR was determined for four separate subjects. The data represent the average of approximately 20 data sets at six time points (480 swallows), and were graphed for the most prominent mid-line structures, the fan-like projecting fibers of the genioglossus throughout the body of the tongue and the vertically projecting fibers of the verticalis in the anterior tongue. Statistical comparisons were made employing the student's t-test of the mean FASR patterns existing in each anatomical region at each time point. Error bars were determined by propagating the deviation of 1D phase-contrast data (Appendix A).

2.5. Experimental protocol

DTI tractography and PC MRI were obtained in the same subjects in separate imaging sessions employing the techniques described above. Data was acquired using a 1.5 T. Siemens Avanto whole-body scanner equipped with two custom-built surface coils, approximately 150 mm^2 in area, placed on each cheek and gently secured with tape. For the acquisition of phase-contrast data, subjects administered 3 ml of water to themselves via a tube connected to a water bladder via a 3 ml syringe. Four swallows were measured for a complete data set, and each time point comprised five averaged data sets. Six time points (0, 100, 200, 300, 400, and 500 ms after gating) were sampled, for a total of 120 swallows. The temporal sequence of phase-contrast data relative to specific time points within the swallow was obtained through the use of lingual pressure gated system, which has been previously validated (Felton et al., 2007). At the onset of the propulsive phase of swallowing, the tip of the tongue involuntarily applies pressure to the hard palate (Nicosia and Robbins, 2001), which is

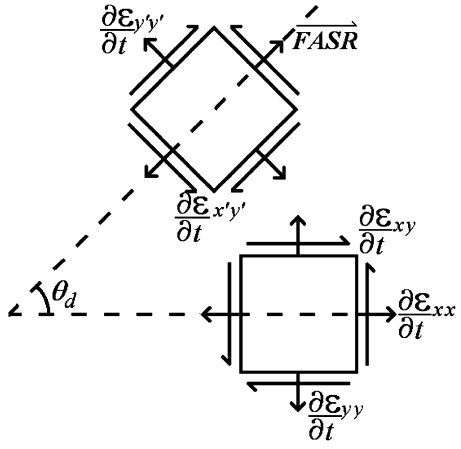

Fig. 2. Derivation of fiber-aligned strain rate (FASR). FASR is defined as the axial strain rate within the reference plane parallel to the maximum diffusion vector. First, the strain rate tensor is measured within the x–y reference plane. $\partial \varepsilon_{xx}/\partial t$ and $\varepsilon_{yy}/\partial t$ are the axial strain rates along the x and y axes, and $\partial \varepsilon_{xy}/\partial t$ is the shear strain rate. It is then transformed via Mohr's circle onto the diffusion-parallel reference plane, and the resulting axial strain rate parallel to the maximum diffusion vector is identified as the FASR. $\partial \varepsilon_{y'y'}/\partial t$ is the other axial strain rate in that reference plane, perpendicular to the maximum diffusion vector, and $\partial \varepsilon_{x'y'}/\partial t$ is the accompanying shear strain rate. FASR is a vector with units s^{-1}.

measured with a bulb sensor (Iowa Oral Performance Instrument, Blaise Medical) (Lazarus et al., 2000). The peak pressure resulting from tongue pressure against the bulb was recorded and a 5 V output signal triggered when a threshold pressure (approximately 0.35 PSI) was achieved. Time points indicated in this manuscript indicate the temporal position in the swallow following the application of the pressure driven trigger pulse.

3. Results

DTI tractography images were generated by determining the maximum diffusion vector per voxel in the mid-sagittal then connecting these vectors based on angular similarity ($<35°$). Fig. 3 displays the tongue at rest in the absence of diffusion weighting (A), as a 3D DTI tractography image (B), and as a 2D rendering of the mid-sagittal component of (B) with a water bolus present. Voxel scale strain rate was determined during swallowing by phase contrast MRI and represented in Lagrangian units of s^{-1} for six time points, each image representing sampling over 80 ms overlaid on the corresponding averaged magnitude images (Fig. 4). The initial application of the tongue to the hard palate (A) is associated with an oblique compression radiating from the bolus to the lower left and lower right, consistent with compression of the palatoglossus and verticalis, along with expansion oriented in the superior and posterior directions, consistent with orthogonal expansion of the palatoglossus tissue or retraction induced by posterior compression of the styloglossus. A prominent oblique compression was observed (consistent with contraction of the genioglossus) at 300 ms (D) and 400 ms (E) with commensurate orthogonal expansion. At 500 ms (F), the tongue exhibited prominent expansion in the distributions of the genioglossus, hyoglossus, and the verticalis, coinciding pharyngeal bolus delivery.

To display voxel strain rate tensors in a multi-voxel format, tractography was applied to the principal strain rate vectors resulting in the creation of strain rate tracts, which were then overlaid on their corresponding magnitude images at the same six time points depicted in Fig. 5. At 0 ms (A) strain rate tracts extend from the bolus obliquely to the anterior of the tongue, and inferior, along the general path of the verticalis and palatoglossus, respectively. In addition, there are orthogonal expansion tracts throughout the tongue. Notably, at 300 ms (D), obliquely aligned strain rate tracts originate in the anterior-inferior portion of the tongue where the mandibular attachment of the genioglossus is located, and fan out in the posterior and superior directions. There are additional compressive tracts consistent with geniohyoid (anterior inferior, obliquely aligned), the hyoglossus (posterior inferior, obliquely aligned) and palatoglossus (posterior superior, vertically aligned). Compressive tracts aligned with the genioglossus, geniohyoid, and hyoglossus were observed at 400 ms (E), including those aligned with the genioglossus, geniohyoid, and hyoglossus. The image obtained at 500 ms (F) shows generalized expansive tract behavior through most of the tongue body.

Fig. 6 displays an arbitrary voxel studied through the process of combining DTI and PC MRI data to calculate FASR, whereas FASR is displayed in Fig. 7 for a single subject during a swallow. The fibers are portrayed as red (compression) or blue (expansion) with hue proportional to magnitude. At 0 ms (A), compression can be seen in tracts consistent with the verticalis and the palatoglossus, as well as radially aligned expansion. The images obtained at 100 (B) and 200 (C) ms show similar strain rate events, but in slowly decreasing magnitude. At 300 ms (D) compression in the apparent distribution of the genioglossus and palatoglossus occurs along with expansion in the distribution of the geniohyoid and verticalis. And 400 ms (E) additionally demonstrates bulk longitudinal shortening of the tongue with initial bolus exposure to the pharynx. Also 500 ms (F) shows expansion throughout the tracts, along with isolated voxels of compression in the verticalis and the genioglossus. Mean FASR was determined for the fan-like

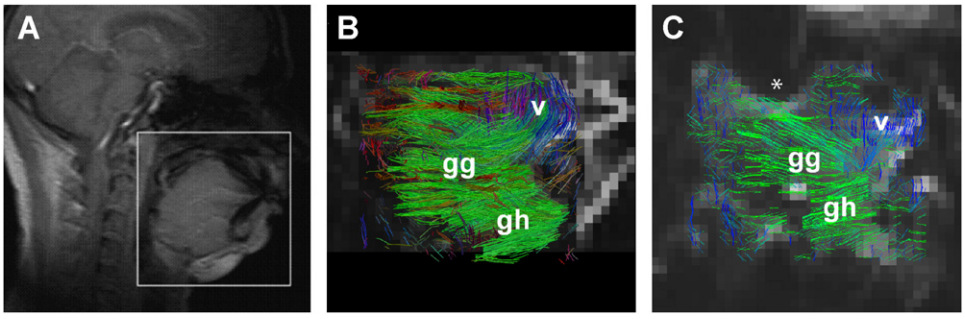

Fig. 3. DTI tractography of the human tongue. DTI tractography images were generated by determining the maximum diffusion vector per voxel then associating these vectors on the basis of angular similarity. Depicted are a sagittal view of the human tongue at rest in the absence of diffusion weighting (A), 3D DTI tractography image of the tongue without the bolus present (B), and a 2D rendering (C) of the 3D data set obtained by deriving the sagittal component (6 mm thick, two slices) of the set of maximum diffusion vectors. The latter represents the explicit structural template used for relating the local strain rate tensor for each subject in this manuscript. These images display principally a vertically aligned set of fibers in the anterior tongue (verticalis, v), an anterior-to–posterior fan-like structure (genioglossus, gg) and a set of fibers connecting the mandible and the hyoid (geniohyoid, gh). Green indicates longitudinally aligned tracts, blue indicates vertically aligned tracts, and red indicates transversely aligned tracts (not shown in the current figure). The asterisk represents the approximate location of the water bolus in (C).

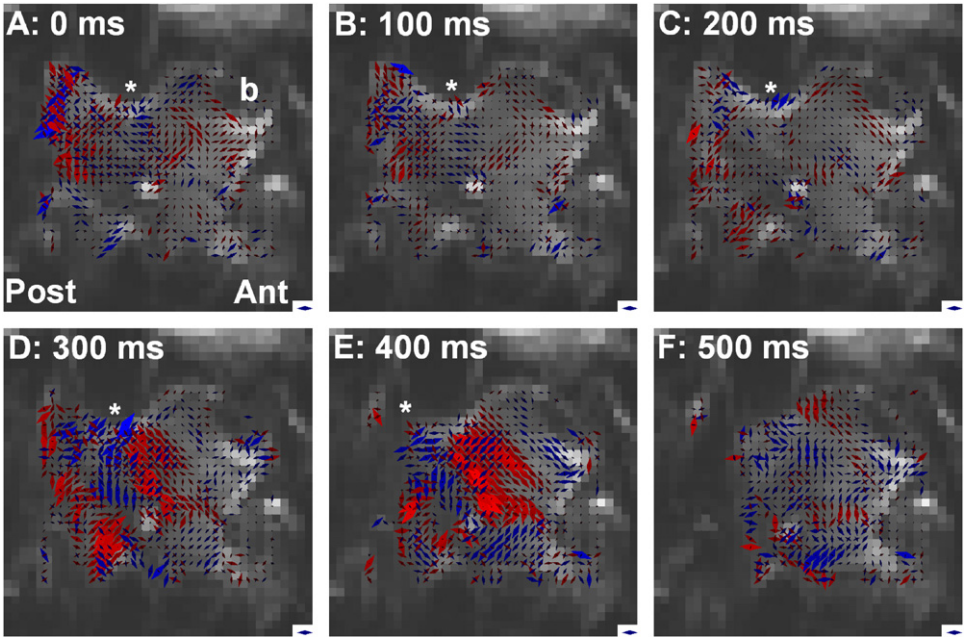

Fig. 4. Strain rate patterns exhibited by the tongue during bolus propulsion. Strain rate tensors were derived in a sagittal image slice using PC MRI for a set of voxels comprising the tongue during the propulsive phase of a 3.0 ml water bolus swallow. Each image was compiled by averaging two simultaneous slices, comprising five sets of strain rate data each, acquired from 20 swallows total. Principal strain rates within each voxel are shown graphically as rhombi with a long axis parallel to the principal strain rate vector, length and hue proportional to the magnitude of the strain rate, and color indicating expansion (blue) or compression (red). For each voxel, two orthogonally aligned rhombi are representative for the primary and secondary strain rate. Shown in this figure is a sequence of six images obtained from a single subject at (A) 0, (B) 100, (C) 200, (D) 300, (E) 400, and (F) 500 ms from the application of the gating pulse. The most prominent events included an obliquely aligned compression (consistent with genioglossus contraction) and orthogonal expansion at approximately 300 and 400 ms followed by expansion in the distributions of the genioglossus, hyoglossus, and the verticalis, coinciding with the deformative pattern occurring during bolus displacement to the oropharynx. The strain rate icon displayed for scale in the lower left of each image represents 0.33 s^{-1}. The asterisk represents the approximate location of the water bolus at the indicated time point. The designation b shown in (A) indicates the position of the pressure-sensing bulb. The lower left image is a T1-weighted MRI image, and indicates the region of the head included in the phase contrast measurement.

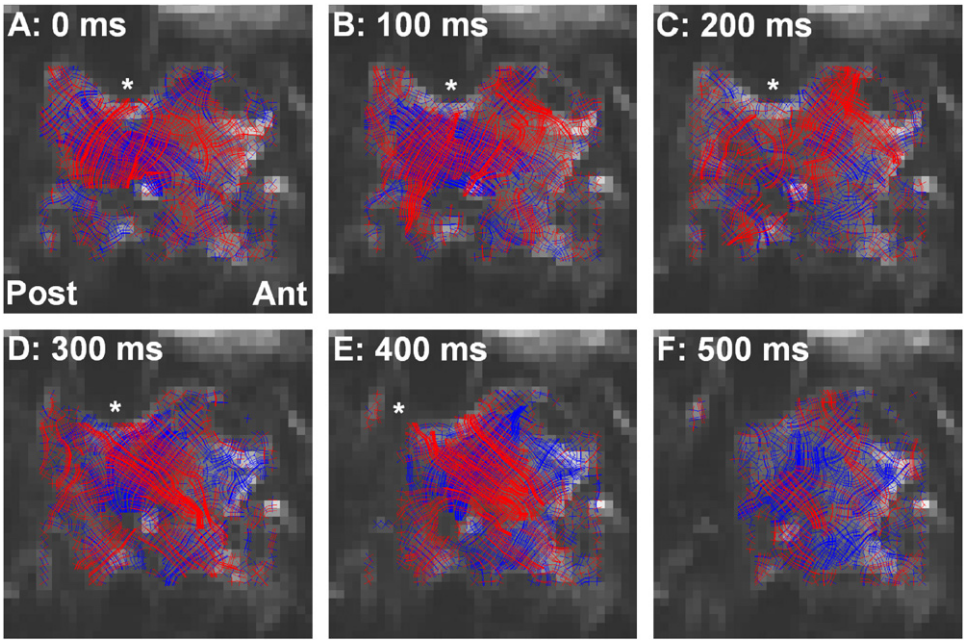

Fig. 5. Strain rate tractography of the tongue during bolus propulsion. Strain rate tensors were derived in a sagittal image slice using PC MRI for a set of voxels comprising the tongue during 3.0 water bolus swallows as described in the legend for Fig. 3. Adjacent and similarly aligned (angle difference less than 35°) principal strain rate vectors were associated via tractography, representing a mesoscale rending of the mechanical events occurring within the tongue during the indicated phase of swallowing. The asterisk represents the approximate location of the water bolus at the indicated time point.

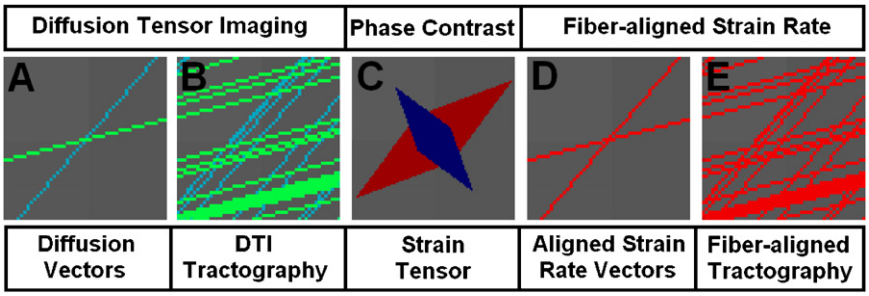

Fig. 6. Demonstration of fiber-aligned strain rate (FASR) for a single voxel. FASR was derived from the relationship between the principal diffusion and strain rate tracts, and displayed in the case of an individual voxel: (A) maximum diffusion vectors of the two-midsagittal slices derived from DTI, (B) display of the same voxel following the application of tractography, (C) strain rate tensor defining two orthogonal principal strain rate vectors, (D) generation of FASR vectors based on the axial strain rate parallel to the maximum diffusion vector within the reference plane with primary axis parallel to the diffusion vector, and (E) tractography rendering of the FASR.

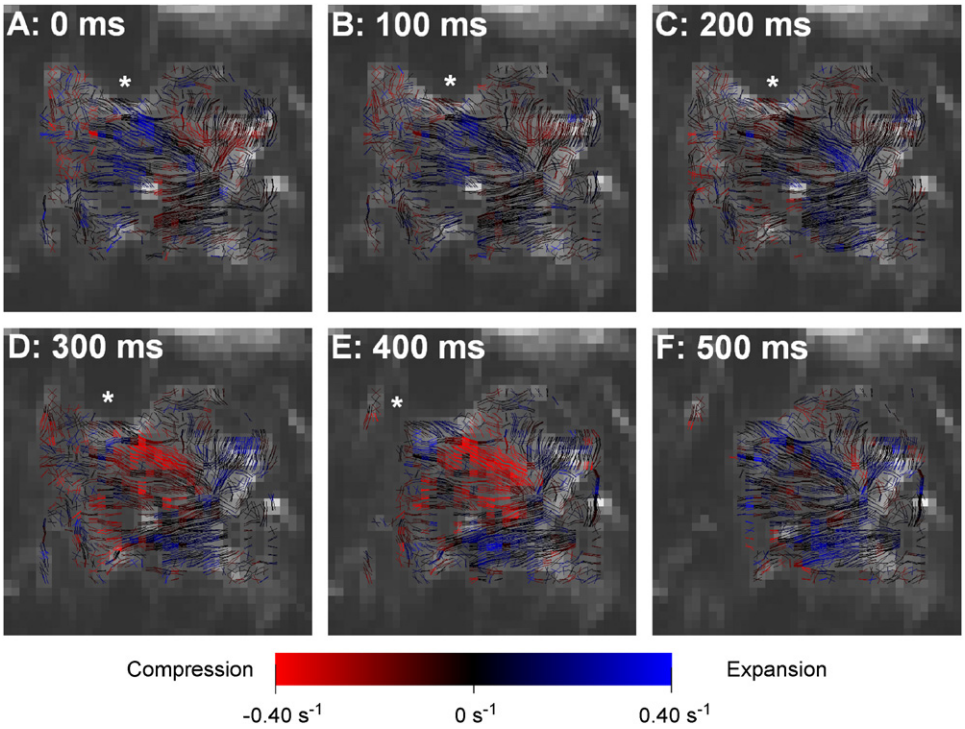

Fig. 7. Fiber-aligned strain rate (FASR) within the human tongue during propulsion. FASR representation of the local mechanical events occurring within the mid-sagittal plane of the tongue during water bolus swallows for single subject as described in the legend for Fig. 3. The hue of these tracts represents the magnitude of the co-located strain rate tensors and their alignment with the diffusion vectors. Each image was compiled by averaging two simultaneous slices, comprising five sets of strain rate data each, acquired from 20 swallows total. We demonstrate significant compression in the distribution of the genioglossus and expansion in the distribution of the geniohyoid and verticalis at 300 ms followed by prominent expansions throughout the tissue leading to net reconfiguration of the tongue during bolus delivery. The asterisk represents the approximate location of the water bolus at the indicated time point.

projecting fibers consistent with the genioglossus and the vertically projecting fibers consistent with the verticalis and depicted in Fig. 8. A distinct pattern was demonstrated whereby initial expansion of the genioglossus (approximately $0.09\,s^{-1}$) converted significantly ($p<0.05$) to compression (approximately $-0.13\,s^{-1}$) maximally at 300 ms, and initial compression of the verticalis (approximately $-0.09\,s^{-1}$) converted to prominent expansion (approximately $0.07\,s^{-1}$) maximally at 400 ms. This time point coincided with initial displacement posterior of the bolus and opening of the oropharynx.

4. Discussion

Resolving the structural underpinnings of local deformation requires a method to quantitatively associate 3D fiber orientation with the local strain rate function. We have previously employed diffusion-weighted MRI methods, which define fiber organization as an array of elements representing directional differences of molecular displacement (Wedeen et al., 2001; Napadow et al., 2001; Gilbert et al., 2006a; Gaige et al., 2007), to image lingual myoarchitecture. The association of diffusion derived vector

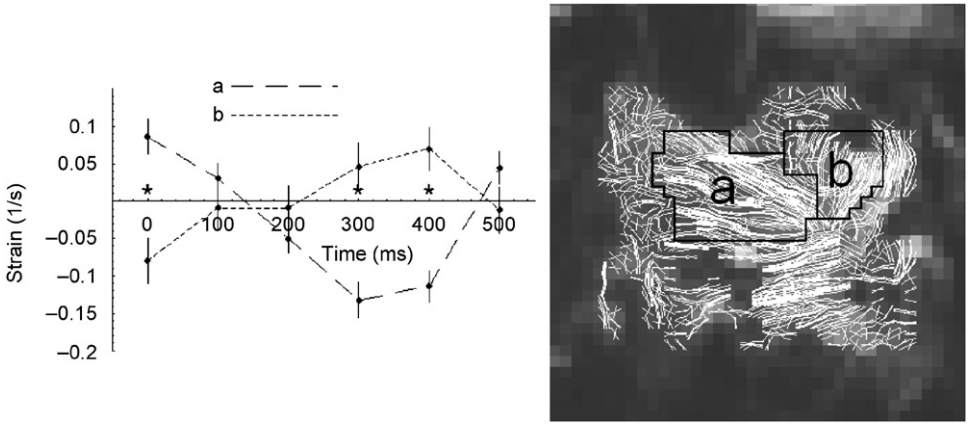

Fig. 8. Region-specific FASR within the tongue during liquid bolus propulsion. The average FASR within the fiber groups consistent with the superior genioglossus (A) and the verticalis (B) were graphed over the six time points during the water bolus swallow. Each data point represents the combined FASR data obtained from each voxel in the region at each time point, and is comprised of five complete data sets from each of four subjects (total of 20 complete data sets). The fibers consistent with the genioglossus display maximum expansion at 0 ms varying to maximum compression 300 ms, whereas the fiber consistent with the verticalis display maximum compression at 0 ms and reach a maximum expansion at 400 ms.

fields with similar alignment from voxel to voxel was used to derive a multi-voxel, fiber-like construct hypothesized to comprise a structural template for fiber shortening (Gilbert et al., 2006b). In order to resolve the spatially and temporally complex mechanical events occurring during human swallowing, we adapted PC MRI methods (Dou et al., 2003; Ebbers et al., 2002; Wedeen et al., 1995) to derive strain rate for the deforming tongue (Felton et al., 2007). These results demonstrated that the propulsive phase of swallowing involves a stereotypical set of compressive and expansive strain rate events resulting from contractions of the intrinsic and extrinsic muscle fibers. We propose herein a method, which relates the direction and magnitude of the diffusion weighted and phase-contrast vectors to yield a metric, termed FASR, in which strain rate parallel to the underlying diffusion vector is obtained. The FASR vector represents the elongation or shortening of the underlying fiber. FASR may indicate either active strain, that deformation which is caused by contraction (or relaxation) of the co-aligned fibers, or passive strain, which is caused by external forces acting on the local tissue.

The current results allow us to extend previous concepts of lingual mechanical function during swallowing by delineating the contribution of specific myofiber tracts. The FASR data reveals that bolus formation and propulsion is the result of synchronized contraction among several lingual fiber populations, notably: (1) Formation of the bolus occurs within the first 200 ms after the gating pulse, and is associated with compression of the verticalis and palatoglossus and expansion in the distribution of the genioglossus. (2) The bolus is displaced to the pharynx at 300–400 ms after the gating pulse due to compression in the distribution of the genioglossus along with expansion in the verticalis and palatoglossus. (3) At 500 ms, there is expansion along all fiber tracts, with isolated voxels of compression, indicative of the passing of the bolus and re-establishment of a relaxed state. These results confirm the relevance of synergies involving intrinsic and extrinsic muscles in the generation of physiological deformations during bolus propulsion (Napadow et al., 1999b, 2002). Such muscular synergy may have functional significance since it allows the species to adapt during swallowing to varying bolus conditions, such as volume or bolus consistency, by modulating the activity of various extrinsic and intrinsic fibers (Thexton and Hiiemae, 1997; Thexton and McGarrick, 1994; Hiiemae and Palmer, 1999) and hyoid displacement (Thexton et al., 2007). Given the needs of species to carry out rapid and forceful lingual reconfiguration during bolus propulsion, one may postulate mechanical synergisms involving the genioglossus hyoglossus, styloglossus and inferior longitudalis combined with a stiffening effect of lingual core compression.

The depiction of FASR as myofiber tracts allows us to consider the extent to which such diffusion generated myofiber tracts serve as a structural template for local deformation. This question has particular importance in the case of the tongue, where the existence of intrinsic–extrinsic overlap complicates the delineation of structure–function relationships. The demonstration of higher FASR values in the apparent distribution of known muscle fiber populations asserts the prominence of these muscles in the indicated deformations. For example, based on the current analysis, it can be argued that contraction of the genioglossus throughout its distribution in combination with relaxation in the distribution of the verticalis and palatoglossus contributes principally to the reconfiguration of the tongue during propulsion. The assignment of a specific structure–function association in the current system is based in on the presence of strain rate in the distribution of a DTI tractography-delineated set of myofiber tracts. We propose that this method provides a basis by which fiber orientation and local deformation can be determined in any such tissue possessing variably aligned muscle fiber populations.

Since the present method does not unambiguously monitor single fiber motor activity in vivo, it is impossible to prove muscle fiber contraction solely from the presence of aligned compression. Moreover, it should be acknowledged that our method associates strain rate data obtained during motion with aligned with DTI tractography data obtained when the tongue is motionless, It is reasonable to presume that some variation of tissue myoarchitecture will result from the tissue deformation itself. The extent that this effect may confer error on aligned strain rate was not addressed in the current study. The present study was confined to the assessment of mid-sagittal mechanics for simplification, although cross-planar strain rate events in also possible given the hydrostatic nature of lingual tissue. Nonetheless, the delineation of strain rate aligned with its myoarchitecture portrayed in this study demonstrates that lingual shape changes during bolus propulsion involve the closely integrated mechanical actions of intrinsic and extrinsic muscles, whose contractility is oriented by the tissue's underlying fiber organization.

Conflict of interest statement

Each author certifies that he has no conflict of interest with any data or material presented in the current manuscript.

Appendix A. Supplementary materials

Supplementary data associated with this article can be found in the online version at doi:10.1016/j.jbiomech.2008.01.030.

References

Basser, P.J., Mattiello, J., LeBihan, D., 1994. MR diffusion tensor spectroscopy and imaging. Biophysics Journal 66, 259–267.

Dou, J., Tseng, W.Y., Reese, T.G., Wedeen, V.J., 2003. Combined diffusion and strain MRI reveals structure and function of human myocardial laminar sheets in vivo. Magnetic Resonance Method 50 (1), 107–113.

Ebbers, T., Wigstrom, L., Bolger, A.F., Wranne, B., Karlsson, M., 2002. Noninvasive measurement of time-varying three-dimensional relative pressure fields within the human heart. Journal of Biomechanical Engineering 124 (3), 288–293.

Felton, S.M., Gaige, T.A., Reese, T.G., Wedeen, V.J., Gilbert, R.J., 2007. Mechanical basis for lingual deformation during the propulsive phase of swallowing as determined by phase-contrast magnetic resonance imaging. Journal of Applied Physiology 103 (1), 255–265.

Gaige, T.A., Benner, T., Wang, R., Wedeen, V.J., Gilbert, R.J., 2007. Three dimensional myoarchitecture of the human tongue determined in vivo by high resolution diffusion tensor imaging with tractography. Journal of Magnetic Resonance Imaging 26 (3), 654–661.

Gilbert, R.J., Magnusson, L.H., Napadow, V.J., Benner, T., Wang, R., Wedeen, V.J., 2006a. Mapping complex myoarchitecture in the bovine tongue with diffusion spectrum magnetic resonance imaging. Biophysics Journal 91 (3), 1014–1022.

Gilbert, R.J., Wedeen, V.J., Magnusson, L.H., Benner, T., Wang, R., Dai, G., Napadow, V.J., Roche, K.K., 2006b. Three-dimensional myoarchitecture of the bovine tongue demonstrated by diffusion spectrum magnetic resonance imaging with tractography. The Anatomical Record Part A: Discoveries in Molecular, Cellular, and Evolutionary Biology 288 (11), 1173–1182.

Gilbert, R.J., Napadow, V.J., Gaige, T.A., Wedeen, V.J., 2007. Anatomical basis of lingual hydrostatic deformation. Journal of Experimental Biology 210 (23), 4069–4082.

Hiiemae, K.M., Palmer, J.B., 1999. Food transport and bolus formation during complete feeding sequences on foods of different initial consistency. Dysphagia 14, 31–42.

Lazarus, C.L., Logemann, J.A., Pauloski, B.R., Rademaker, A.W., Larson, C.R., Mittal, B.B., Pierce, M., 2000. Swallowing and tongue function following treatment for oral and oropharyngeal cancer. Journal of Speech Language Hearing Research 43 (4), 1011–1023.

Napadow, V.J., Chen, Q., Wedeen, V.J., Gilbert, R.J., 1999a. Intramural mechanics of the human tongue in association with physiological deformations. Journal Biomechanics 32, 1–12.

Napadow, V.J., Chen, Q., Wedeen, V.J., Gilbert, R.J., 1999b. Biomechanical basis for lingual tissue deformation during swallowing. American Journal Physiology 40, G695–G701.

Napadow, V.J., Chen, Q., Mai, V., So, P.T.C., Gilbert, R.J., 2001. Quantitative analysis of 3D resolved fiber architecture in heterogeneous skeletal muscle using NMR and optical imaging methods. Biophysics Journal 80, 2968–2975.

Napadow, V.J., Kamm, R.D., Gilbert, R.J., 2002. Biomechanical model of sagittal bending for the human tongue. Journal of Biomechanical Engineering 124, 547–556.

Nicosia, M.A., Robbins, J.A., 2001. The fluid mechanics of bolus ejection from the oral cavity. Journal of Biomechanics 34 (12), 1537–1544.

Smith, K.K., 1986. Morphology and function of the tongue and hyoid apparatus in Varanus (Varanidae, Lacertilia). Journal of Morphology 187, 261–287.

Smith, K.K., Kier, W.M., 1989. Trunks, tongues, and tentacles: moving with skeletons of muscle. American Scientist 77, 29–35.

Sonntag, C.F., 1925. The comparative anatomy of the tongues of mammalia. XII. Summary, classification, and physiology. Journal of Zoological Proceedings of the Zoological Society London 21, 701–762.

Stejskal, E., Tanner, J., 1965. Use of spin echoes in a pulsed magnetic field gradient to study anisotropic restricted diffusion and flow. Journal of Chemical Physics 43, 3597–3603.

Thexton, A., Hiiemae, K.M., 1997. The effect of food consistency upon jaw movement in the macaque: a cineradiographic study. Journal of Dental Research 76, 552–560.

Thexton, A.J., McGarrick, J.D., 1994. The electromyographic activities of jaw and hyoid musculature in different ingestive behaviors in the cat. Archivs of Oral Biology 39, 599–612.

Thexton, A., Crompton, A.W., German, R.Z., 2007. Electromyographic activity during the reflex pharyngeal swallow in the pig: Doty and Bosma (1956) revisited. Journal of Applied Physiology 102 (2), 587–600.

Wedeen, V.J., Weisskoff, R.M., Reese, T.G., Beache, G.M., Poncelet, B.P., Rosen, B.R., Dinsmore, R.E., 1995. Motionless movies of myocardial strain-rates using stimulated echoes. Magnetic Resonance Method 33 (3), 401–408.

Wedeen, V.J., Reese, T.G., Napadow, V.J., Gilbert, R.J., 2001. Demonstration of primary and secondary fiber architecture of the bovine tongue by diffusion tensor magnetic resonance imaging. Biophysics Journal 80, 1024–1028.